Journal of Thermal Biology 86 (2019) 102430

Contents lists available at ScienceDirect

Journal of Thermal Biology

journal homepage: http://www.elsevier.com/locate/jtherbio

Numerical analysis of power dissipation requirement in magnetic hyperthermia problems

Kuo-Chi Liu *, Po-Jen Cheng

Department of Mechanical Engineering, Far East University, 49 Chung Hua Rd, Hsin-Shih, Tainan, 744, Taiwan

ARTICLE INFO

Keywords:
Bi-layered solid sphere
Hyperthermia
Laplace transform
Power dissipation

ABSTRACT

Control of the therapeutic temperature is essential in performing magnetic fluid hyperthermia. Thus, reliable predictions of the power dissipation are required to determine the correct dosage of magnetic particles to be injected into the cancerous tissue prior to treatment. To meet this requirement, the present study evaluates the power dissipation requirement for two magnetic hyperthermia problems reported in the literature. There is a significant challenge for solving the bio-heat transfer model for concentric bi-layered solid spheres. Consequently, the present study employs a hybrid technique based on Laplace transformation and a modified discretization scheme to solve the considered hyperthermia problems. Analytical solutions are provided to demonstrate the validity of the proposed approach. The unreliability of the results presented in the literature is then demonstrated using the proposed numerical scheme. In general, the results presented in this study show that the power dissipation required to maintain an effective temperature range in the tumor domain is related to the rate of temperature rise, the tumor size, the blood perfusion rate, and the tissue properties. In particular, the power dissipation should be increased for the cooling effect of blood perfusion or a smaller tumor volume.

1. Introduction

It has been reported that the growth of cancerous cells can be terminated by heating the affected organ or tissue to a temperature in the range of 42–46 °C (Hervault and Thanh, 2014; Chiriac et al., 2015). This phenomenon was first exploited by Gilchrist et al., (1957), who developed a technique referred to as magnetic hyperthermia for oncology applications. Magnetic hyperthermia involves increasing the cell temperature via the heat dissipation produced by magnetic particles exposed to a high-frequency alternating magnetic field (Lahiri et al., 2016). It has achieved remarkable success in clinical trials for prostate cancer and glioma treatment (Johannsen et al., 2007; Johannsen et al., 2010), and is virtually free of patient discomfort or side effects. However, further improvements are still required before it can enter mainstream clinical practice. One of the most important problems to be addressed is that of determining the proper amount of magnetic particles to be injected into the tumor prior to treatment and then maintaining the tumor tissue at the required temperature as the treatment process proceeds (Thiesen and Jordan, 2008).

With the development of nanotechnology, the potential of magnetic fluid hyperthermia for therapeutic applications has attracted significant attention in recent years. Lahiri et al., (2016) examined the effects of the initial susceptibility and size polydispersity of phosphate-coated iron oxide nanoparticles on the magnetic hyperthermia efficiency given a constant excitation frequency of 126 kHz and various sample concentrations and external field amplitudes. Hedayatnasab et al., (2017) reviewed the surface chemistry, intrinsic, and extrinsic magnetic properties of various magnetic nanoparticles used in hyperthermia therapy. Wu and Wang (2017) investigated the optimal magnetic field strength and frequency for maximizing the power generation rate of various magnetite nanoparticle assemblies in hyperthermia applications. Tang et al., (2018) explored the effect of the infusion rate and diffusion duration of magnetic particles on the efficiency of magnetic hyperthermia treatment. Cobianchi et al., (2017) performed an experimental investigation into the main physical properties affecting the heat release capability of maghemite nanoparticles with different core diameter sizes. Chen et al., (2018) utilized a thermal transport model to examine the effects of the nanoparticle concentration, nanoparticle magnetization, magnetic field strength and magnetic field frequency on the temperature induced in hyperthermia treatment. Lyutyy et al., (2019) employed analytical and numerical techniques to approximate the limits of the heating rate in magnetic fluid hyperthermia. Das et al., (2019) reviewed the current progress in the development of magnetic

* Corresponding author.
E-mail address: kcliu@mail.feu.edu.tw (K.-C. Liu).

https://doi.org/10.1016/j.jtherbio.2019.102430
Received 18 April 2019; Received in revised form 3 October 2019; Accepted 4 October 2019
Available online 6 October 2019

Nomenclature

A	area of boundary surface, m^2
a	radius of tissue, m
c	specific heat of tissue, J/kg· K
c_b	specific heat of blood, J/kg· K
f	parameter defined in Eq. (26)
k	thermal conductivity, W/m· K
P	power density, W/m^3
q	heat flux, W/m^2
q_m	metabolic heat generation rate, W/m^3
r	space coordinate, m
R	radius of tumor, m
s	Laplace transform parameter
t	time, s
T	temperature of tissue, °C
T_b	arterial temperature, °C
T_o	initial temperature of tissue, °C
w_b	perfusion rate of blood, 1/s

Greek symbols

θ	new dependent variable, $\theta = r(T - T_0)$
$\tilde{\theta}$	Laplace transform of θ
λ	parameter defined in Eq. (25)
ρ	density, kg/m^3
ψ	volume fraction of magnetic particles
τ	relaxation time, s

Subscripts

mp	magnetic particle
tt	tumor tissue

nanoparticle hyperthermia therapy and examined some of the fundamental issues involved in developing effective magnetic nanoparticle heat mediators for practical clinical contexts.

In implementing magnetic fluid hyperthermia, one of the most challenging problems is that of maintaining an appropriate temperature in the treatment region. Therefore, analyzing the underlying thermal mechanisms involved in the hyperthermia treatment process such that the temperature distribution in the affected region can be accurately determined is essential in ensuring the success of the therapeutic procedure (Zhou et al., 2007). Various bio-heat transfer models have been developed in recent years. For example, Liu et al., (2016) used a dual-phase-lag model to investigate the heat conduction behavior in biological tissues. Liu and Chen (2018) developed a generalized dual-phase-lag bio-heat transfer model to explore the effect of the transient blood temperature on the power dissipation rate required to maintain the tumor at the appropriate treatment temperature. Dutta and Kundu (2018) developed exact analytical models for the temperature distribution in single-layered biological tissues using Fourier and non-Fourier heat transfer approaches, respectively. The authors in (Bagaria and Johnson, 2005; Maenosono and Saita, 2006; Tang et al., 2017; Wu et al., 2015) used the Pennes heat bio-transfer equation to predict the tissue temperature in magnetic fluid hyperthermia based on the assumption of a concentric bi-layered solid sphere consisting of a small amount of tumor material surrounded by a large amount of healthy tissue. Tang et al., (2017) developed a finite element method for determining the critical power dissipation of magnetic particles which maximized the effectiveness of the hyperthermia procedure while ensuring that the local temperature did not exceed the prescribed therapeutic range. Wu et al., (2015) simulated the temperature distribution in the tumor region during hyperthermia therapy using a bi-layered spherical model with blood perfusion and metabolism heating effects.

Tang et al., (2017) and Wu et al., (2015) both used finite element analysis methods to solve the bio-heat transfer problem in magnetic hyperthermia. However, a close inspection of (Tang et al., 2017) reveals apparent contradictions in the values reported for the temperature variation within the tumor domain. Similarly, the calculation results presented in (Wu et al., 2015) for the edge temperature are inconsistent with the adopted boundary condition. In practice, a reliable and rational prediction of the power dissipation is essential in improving the safety and effectiveness of magnetic hyperthermia therapy. Accordingly, the present study employs a hybrid method based on the Laplace transform technique and a modified discretization scheme (Liu and Cheng, 2008) to solve the same problems as those reported in Tang et al., (2017) and Wu et al., (2015). Analytical solutions are additionally derived to demonstrate the validity of the present results. Finally, the power dissipation required to achieve an effective temperature range in the tumor domain is estimated for various statuses.

2. Mathematical formulation

Tang et al., (2017) and Wu et al., (2015) modeled the magnetic hypothermia treatment area as a solid bi-layered sphere with constant heat generation and used the Pennes bio-heat transfer equation to describe the heat flow from the tumor domain to the healthy tissue domain. It was assumed that the tumor contained a homogeneous distribution of magnetic particles which produced a spherical heat source with a constant power density P under excitation by a high-frequency alternating magnetic field. In addition, the heat produced by the heat source was assumed to transfer symmetrically in the radial direction. Consequently, the temperature distribution in the tumor and surrounding healthy tissue varied as a function of both the distance r from the center of the sphere and the time t.

In the present study, the tumor and normal tissues are assumed to have constant physiological parameters and the heat transfer in the tumor and normal tissue domains are modeled respectively as

$$\rho_1 c_1 \frac{\partial T_1}{\partial t} = k_1 \frac{1}{r^2}\frac{\partial}{\partial r}\left(r^2 \frac{\partial T_1}{\partial r}\right) + w_{b1}\rho_b c_b (T_b - T_1) + q_{m1} + P \quad \text{for} \quad 0 \le r \le R, \tag{1}$$

$$\rho_2 c_2 \frac{\partial T_2}{\partial t} = k_2 \frac{1}{r^2}\frac{\partial}{\partial r}\left(r^2 \frac{\partial T_2}{\partial r}\right) + w_{b2}\rho_b c_b (T_b - T_2) + q_{m2} \quad \text{for} \quad R \le r \le a. \tag{2}$$

where ρ, c, k and T are the density, specific heat, thermal conductivity and temperature in the two domains, respectively. In addition, ρ_b, c_b and w_b are the density, specific heat and perfusion rate of blood, respectively, while q_m is the metabolic heat generation rate. Finally, T_b is the arterial temperature and is assumed to have a value of 37 °C.

In Eq. (1), the region bounded by $0 \le r \le R$ is a composite region consisting of tumor tissue and magnetic particles. The effective density ρ_1, specific heat c_1 and thermal conductivity k_1 of this composite region can be approximated by a serial arrangement of the two materials with appropriate volume proportions (Tang et al., 2017; Wu et al., 2015), i.e.,

$$\rho_1 = \psi\rho_{mp} + (1-\psi)\rho_{tt}, \tag{3}$$

$$c_1 = \psi c_{mp} + (1-\psi)c_{tt}, \tag{4}$$

$$1/k_1 = \psi/k_{mp} + (1-\psi)/k_{tt}, \tag{5}$$

where subscripts mp and tt denote magnetic particles and tumor tissue,

respectively, and ψ is the volume fraction of magnetic particles.

In (Tang et al., 2017; Wu et al., 2015), the temperature at the edge of the normal tissue was taken as the initial temperature (see below) and the boundary conditions were given as follows:

$$\frac{\partial T_1(0,t)}{\partial r}=0 \text{ and } T_1(0,t) \text{ and is finite,} \tag{6}$$

$$T_1(R,t)=T_2(R,t), \tag{7}$$

$$q_1(R,t)=q_2(R,t) \text{ (or) } k_1\frac{\partial T_1(R,t)}{\partial r}=k_2\frac{\partial T_2(R,t)}{\partial r}, \tag{8}$$

$$T_2(a,t)=T_0. \tag{9}$$

In addition, the initial conditions were set as

$$T_j(r,0)=T_0, \quad \frac{\partial T_j(r,0)}{\partial t}=0, \text{ and } \quad q_j(r,0)=0, \qquad j=1,\ 2. \tag{10}$$

where the initial temperature T_0 was taken as the arterial temperature (i.e., $T_b=37\ ^\circ C$).

3. Analysis

Let a new dependent variable, θ, be defined for transforming the present problem from a spherical coordinate system to a rectangular coordinate system, i.e.,

$$\theta=r(T-T_0). \tag{11}$$

Equations (1) and (2) can be rewritten in terms of variableθas follows:

$$\rho_1 c_1\frac{\partial\theta_1}{\partial t}=k_1\frac{\partial^2\theta_1}{\partial r^2}-w_{b1}\rho_b c_b\theta_1+(q_{m1}+P)r \qquad \text{for } 0\le r\le R, \tag{12}$$

$$\rho_2 c_2\frac{\partial\theta_2}{\partial t}=k_2\frac{\partial^2\theta_2}{\partial r^2}-w_{b2}\rho_b c_b\theta_2+q_{m2}r \qquad \text{for } R\le r\le a. \tag{13}$$

The boundary conditions become

$$\theta_1(0,\ t)=0, \tag{14}$$

$$\theta_1(R,\ t)=\theta_2(R,\ t), \tag{15}$$

$$k_1\left(\frac{\partial\theta_1(R,\ t)}{\partial r}-\frac{\theta_1}{R}\right)=k_2\left(\frac{\partial\theta_2(R,\ t)}{\partial r}-\frac{\theta_2}{R}\right), \tag{16}$$

$$\theta 2(a,\ t)=0. \tag{17}$$

Similarly, the initial conditions are rewritten as

$$\theta_j(r,\ 0)=0, \quad \frac{\partial\theta_j(r,\ 0)}{\partial t}=0, \text{ and } \quad q_j(r,\ 0)=0 \qquad j=1,\ 2. \tag{18}$$

In Eq. (11), the temperature T is equal to $\theta/r+T_0$. The value of θ/r at $r=0$ is indeterminate and must be replaced by its limit as $r\to 0$. In other words, the value of the transient temperature at the center of the tumor region, $T(0,\ t)$, can be evaluated using L'Hôspital's rule as

$$T(0,t)=\lim_{r\to 0}\frac{\theta}{r}+T_0=\frac{d\theta}{dr}+T_0. \tag{19}$$

The transient problem described above can be converted to a steady problem by applying the Laplace transform technique. In particular, the differential heat transfer equations given in Eqs. (12) and (13), respectively, together with the boundary conditions given in Eq. (14)~(17), can be transformed in conjunction with the initial conditions (Eq. (18)) as

$$\frac{d^2\tilde{\theta}_j}{dr^2}-\lambda_j^2\tilde{\theta}_j=-f_j r, \qquad j=1,\ 2 \tag{20}$$

and

$$\tilde{\theta}_1(0,s)=0, \tag{21}$$

$$\tilde{\theta}_1(R,s)=\tilde{\theta}_2(R,s), \tag{22}$$

$$k_1\left(\frac{d\tilde{\theta}_1(R,s)}{dr}-\frac{\tilde{\theta}_1}{R}\right)=k_2\left(\frac{d\tilde{\theta}_2(R,s)}{dr}-\frac{\tilde{\theta}_2}{R}\right), \tag{23}$$

$$\tilde{\theta}_2(a,s)=0, \tag{24}$$

where

$$\lambda_j^2=\frac{1}{k_j}\left(\rho_j c_j s+w_{bj}\rho_b c_b\right), \qquad j=1,\ 2 \tag{25}$$

$$f_1=\frac{q_{m1}+P}{k_1 s}, \tag{26a}$$

$$f_2=\frac{q_{m2}}{k_2 s}. \tag{26b}$$

Note that s is the Laplace transform parameter with respect to t, and $\tilde{\theta}$ is the function θ written in the Laplace domain. In addition, subscript j denotes the layer number.

The interfacial boundary condition between the tumor and healthy tissue layers introduces the complexity and causes some mathematical difficulties when attempting to solve the problem directly in the temperature domain. Thus, this paper does a numerical analysis while the analytical solution in the Laplace transform domain is presented. Then, the inverse procedure is applied to estimate the power dissipation.

3.1. Numerical analysis

For a small control volume, $\tilde{\theta}$ is approximated using nodal temperatures and shape functions. Due to the existence of the derivative term in Eq. (20), the chosen shape function has a significant effect on the accuracy of the numerical results. Hence, in the present study, the shape function is derived from the analytical solution of Eq. (20) in the sub-space domain k, $[r_i, r_{i+1}]$, in the form

$$\tilde{\theta}_{k,j}=\frac{1}{\sinh\lambda_j\ell}\left[\left(\tilde{\theta}_{i,j}-\frac{f_j}{\lambda_j^2}r_i\right)\sinh\lambda_j(r_{i+1}-r)+\left(\tilde{\theta}_{i+1,j}-\frac{f_j}{\lambda_j^2}r_{i+1}\right)\sinh\lambda_j(r-r_i)\right]+\frac{f_j}{\lambda_j^2}r, \qquad i=1,\ 2,....n\ ;\ \ j=1,\ 2;\ k=i \tag{27}$$

Equation (27) can be written in the sub-space domain k-1, $[r_{i-1}, r_i]$, as follows:

$$\tilde{\theta}_{k-1,j}=\frac{1}{\sinh\lambda_j\ell}\left[\left(\tilde{\theta}_{i-1,j}-\frac{f_j}{\lambda_j^2}r_{i-1}\right)\sinh\lambda_j(r_i-r)+\left(\tilde{\theta}_{i,j}-\frac{f_j}{\lambda_j^2}r_i\right)\sinh\lambda_j(r-r_{i-1})\right]+\frac{f_j}{\lambda_j^2}r, \tag{28}$$

where ℓ denotes the length of the sub-space domain or the distance between neighboring nodes. In addition, subscript i denotes the node number and n is the total number of nodes.

For a perfect contact at the interface between the tumor tissue and normal tissue, the heat flux and temperature within the whole space domain are continuous. In other words, the following equalities hold:

$$\tilde{\theta}_{k-1,j}(r_i)=\tilde{\theta}_{k,j}(r_i), \tag{29}$$

$$k_j\left(\frac{d\tilde{\theta}_{k-1,j}(r_i)}{dr}-\frac{\tilde{\theta}_{k-1,j}}{r_i}\right)=k_j\left(\frac{d\tilde{\theta}_{k,j}(r_i)}{dr}-\frac{\tilde{\theta}_{k,j}}{r_i}\right). \tag{30}$$

Substituting Eqs. (27)–(29) into Eq. (30) and evaluating the resulting derivative leads to the following discretized form of $\tilde{\theta}$ at the interior nodes of layer j:

$$\tilde{\theta}_{i-1,j} - 2\cosh(\lambda_j \ell)\tilde{\theta}_{i,j} + \tilde{\theta}_{i+1,j} = \frac{f_j}{\lambda_j^2}\left[r_{i-1} - 2r_i \cosh(\lambda_j \ell) + r_{i+1}\right]. \quad (31)$$

The discretized form of $\tilde{\theta}$ at the node located at the interface between the tumor and normal tissues can be obtained from the boundary condition as

$$k_1\frac{\lambda_1}{\sinh\lambda_1\ell}\tilde{\theta}_{i-1,1} - E_1\tilde{H}_{i,(1,2)} + k_2\frac{\lambda_2}{\sinh\lambda_2\ell}\tilde{H}_{i+1,2} = k_1\frac{1}{\sinh\lambda_1\ell}\frac{f_1}{\lambda_1}(R-\ell) - E_2R + k_2\frac{1}{\sinh\lambda_2\ell}\frac{f_2}{\lambda_2}(R+\ell) + k_1\frac{f_1}{\lambda_1^2} - k_2\frac{f_2}{\lambda_2^2}, \quad (32)$$

where

$$E_1 = k_1\frac{\lambda_1\cosh\lambda_1\ell}{\sinh\lambda_1\ell} + k_2\frac{\lambda_2\cosh\lambda_2\ell}{\sinh\lambda_2\ell} + \frac{k_2}{R} - \frac{k_1}{R}, \quad (33a)$$

$$E_2 = k_1\frac{\cosh\lambda_1\ell}{\sinh\lambda_1\ell}\frac{f_1}{\lambda_1} + k_2\frac{\cosh\lambda_2\ell}{\sinh\lambda_2\ell}\frac{f_2}{\lambda_2}. \quad (33b)$$

Equations (31) and (32), in conjunction with the discretized forms of the boundary conditions, can be rearranged in the following matrix form:

$$[B]\{\tilde{\theta}\} = \{F\}, \quad (34)$$

where $[B]$ is a matrix with complex numbers, $\{\tilde{\theta}\}$ is a column vector in the Laplace transform domain, and $\{F\}$ is a column vector representing the forcing term. The value of θ in the physical domain can then be determined via the application of the Gaussian elimination algorithm followed by numerical inversion of the Laplace transform (Honig and Hirdes, 1984).

3.2. Analytical solution

The analytical solution of Eq. (20) with the related boundary conditions can be written as

$$\widetilde{\theta_1} = C_1(e^{\lambda_1 r} - e^{-\lambda_1 r}) + \frac{f_1}{\lambda_1^2}r \quad \text{for } 0 \le r \le R, \quad (35)$$

$$\widetilde{\theta_2} = C_2\left(e^{-\lambda_2 r} - e^{\lambda_2(r-2a)}\right) + \frac{f_2}{\lambda_2^2}r - \frac{f_2}{\lambda_2^2}\cdot a\cdot e^{\lambda_2(r-a)} \quad \text{for } R \le r \le a, \quad (36)$$

where

$$C_1 = [(N_5+N_6)(N_1+N_2N_7) + N_2N_4N_6]/[N_0N_4 - N_1N_3 - N_2N_3N_7], \quad (37a)$$

$$C_2 = -\frac{N_3N_7}{N_4}C_1 - \frac{N_7}{N_4}(N_5+N_6) - N_6, \quad (37b)$$

$$N_0 = k_1\left[\left(\lambda_1 - \frac{1}{R}\right)e^{\lambda_1 R} + \left(\lambda_1 + \frac{1}{R}\right)e^{-\lambda_1 R}\right], \quad (37c)$$

$$N_1 = k_2\left(\lambda_2 - \frac{1}{R}\right)e^{\lambda_2 R}, \quad (37d)$$

$$N_2 = k_2\left(\lambda_2 + \frac{1}{R}\right)e^{-\lambda_2 R} \quad (37e)$$

$$N_2 = e^{(\lambda_2+\lambda_1)R} - e^{(\lambda 2-\lambda_1)R}, \quad (37f)$$

$$N_4 = e^{2\lambda_2 R} - e^{2\lambda_2 a}, \quad (37g)$$

$$N_5 = \left(\frac{f_1}{\lambda_1^2} - \frac{f_2}{\lambda_2^2}\right)\cdot R\cdot e^{\lambda_2 R}, \quad (37h)$$

$$N_6 = \frac{f_2}{\lambda_2^2}\cdot a\cdot e^{\lambda_2 a}, \quad (37i)$$

and

$$N_7 = e^{2\lambda_2 a}. \quad (37j)$$

It is found from Eqs. (3), (35) and (36)7a)~(37j) that the structure of the analytical solution is complicated. Thus, the numerical inversion of the Laplace transform (Honig and Hirdes, 1984) is again applied to derive the inverse transforms of Eqs. (35) and (36) for θ_1 and θ_2, respectively. The analytical results are then used to evaluate the reliability of the numerical solutions obtained using the method described in Section 3.1 above.

4. Results and discussion

4.1. Problem 1

This section considers the same problem as that studied in (Tang et al., 2017), namely that of estimating the critical power dissipation in the hyperthermia treatment of a tumor within the liver. The relevant properties of the liver, tumor, blood and magnetic nanoparticles are shown in Table 1. The composite values, ρ_1, c_1 and k_1, of the tumor and ferrofluid material were calculated from Eq. (3)~(5) given the assumption of a nanoparticle volume fraction of $\psi = 0.071$. The radii of the tumor and healthy tissue regions of the bi-layered spherical model were set as $R = 18$ mm and $a = 40$ mm, respectively (Tang et al., 2017).

To simplify the problem, Tang et al., (2017) ignored the effects of vascularization and blood perfusion in the tumor domain. The authors indicated that in the no blood vessel model (NBVM), the maximum temperature occurred at the center of the tumor region and reduced rapidly to 37 °C at the edge of the tumor domain under steady-state conditions given a power density of $P = 7{\cdot}10^6 \mathrm{W/m^3}$. However, as shown in Fig. 1 (reproduced from Fig. 6(b) in (Tang et al., 2017)), the steady state temperature at the edge of the tumor is actually closer to 41 °C. In other words, a contradiction exists between the assumed temperature at the edge of the tumor domain and the calculated temperature.

From an energy conservation perspective, the heat loss through the boundary surface at $r = a$ should equal the sum of the power dissipation and metabolism heat required to maintain a steady-state condition in the NBVM. From the principle of heat conduction, the heat loss through the boundary surface can be approximated as

$$k_2 A\frac{\mathrm{d}T}{\mathrm{d}r} \approx k_2\cdot 4\cdot\pi\cdot a^2\frac{(T_R - T_0)}{(a-R)} = 0.59\cdot 4\cdot\pi\cdot(0.04)^2\frac{(T_R - 37)}{0.022}, \quad (38)$$

where T_R is the temperature at the edge of the tumor domain and A is the area of the boundary surface. Furthermore, the sum of the power dissipation ($P = 7{\cdot}10^6 \mathrm{W/m^3}$) and metabolism heat produced by the tumor and healthy tissue can be estimated as

Table 1
Values of relevant parameters for problem considered in (Tang et al., 2017).

Parameters	Liver	Tumor	Blood	Magnetite
Density [kg/m^3]	1064	1060	1050	5180
Thermal conductivity [W/m K]	0.59	0.52	0.51	40
Specific heat [J/kg K]	4180	3540	4180	670
Metabolic heat generation [W/m^3]	684	5790	–	–

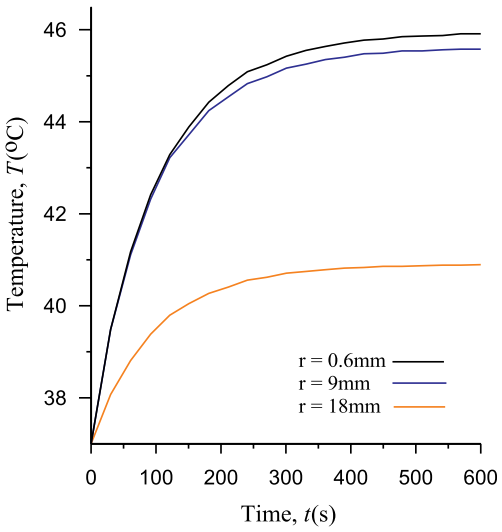

Fig. 1. Calculation results for temperature variation at various locations within tumor given power dissipation of $P = 7{\cdot}10^6\mathrm{W/m^3}$ (Note that the figure is reproduced from Fig. 6(b) in (Tang et al., 2017).).

$$\begin{aligned}&(P+q_{m1})\cdot\frac{4}{3}\pi\cdot R^3+q_{m2}\cdot\frac{4}{3}\pi\cdot\left(a^3-R^3\right)\\&=\left(7{\cdot}10^6+5790\right)\cdot\frac{4}{3}\pi\cdot(0.018)^3+684\cdot\frac{4}{3}\pi\cdot\left(0.04^3-0.018^3\right).\\&=170.84(\mathrm{W})\end{aligned}\tag{39}$$

As a result,

$$0.59{\cdot}4{\cdot}\pi\cdot(0.04)^2\frac{(T_R-37)}{0.022}\approx 170.84(\mathrm{W}).\tag{40}$$

It is seen from Eq. (40) that the temperature at the edge of the tumor domain reaches approximately 350 °C at the steady state. This result evidences the temperature trend shown in Fig. 2, which presents the numerical and analytical results obtained for the time-based variation of the temperature at various positions within the tumor tissue given an assumed power dissipation of $P = 7{\cdot}10^6\mathrm{W/m^3}$, is rational. Notably, a good agreement is observed between the analytical solution for the temperature variation at each of the considered positions within the tumor tissue and the numerical solution. Consequently, the validity of the present numerical method is confirmed.

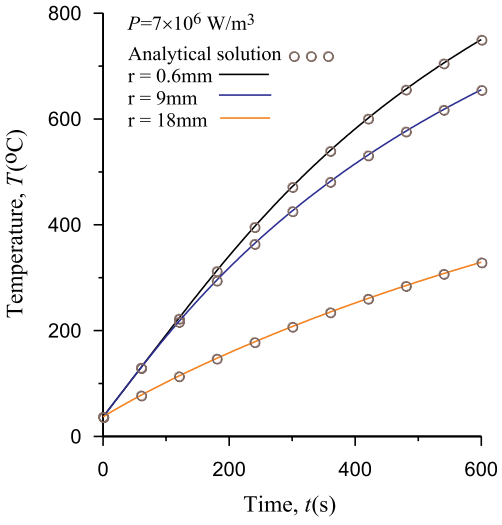

Fig. 2. Comparison of present numerical and analytical results for problem considered in (Tang et al., 2017).

In general, the critical power dissipation in magnetic hyperthermia is set in such a way as to increase the tumor temperature without exceeding the maximum temperature defined for treatment (typically around 42–46 °C (Hervault and Thanh, 2014; Chiriac et al., 2015)). According to the results presented in (Tang et al., 2017), the temperature at the edge of the tumor domain is around 41 °C. Thus, the authors claimed that the specified power dissipation of $P = 7{\cdot}10^6\mathrm{W/m^3}$ represents the critical power dissipation. However, the present results indicate that a power density of $P = 7{\cdot}10^6\mathrm{W/m^3}$ is actually far too high for safe hyperthermia.

Fig. 1 indicates that the temperature within the tumor region reaches an effective magnetic hyperthermia treatment temperature of 42 °C after around 75 s of excitation at locations $r = 0.6$ mm and $r = 9$ mm. However, in the present study, the power dissipation required to achieve T (0.6 mm, 75 s) = 42 °C was determined to be $P = 2.9519{\cdot}10^5\mathrm{W/m^3}$ (i.e., much lower than the power dissipation of $P = 7{\cdot}10^6\mathrm{W/m^3}$ assumed in Fig. 1.) through an inverse procedure. Under such conditions, the temperature distribution did not reach steady state even after $t = 600$ s (see Fig. 3). Moreover, the temperatures at $r = 0.6$ mm and $r = 18$ mm were found to be 67.65 °C and 49.61 °C, respectively. These results are clearly very different from those presented in Fig. 1. However, they are confirmed by the present analytical method. Consequently, the reliability of the results presented in Fig. 1 (reproduced from (Tang et al., 2017)) is in significant doubt. Furthermore, the present results suggest that increasing the computational complexity (as in (Tang et al., 2017)) does not necessarily guarantee an improved accuracy of the calculation results.

To explore the effect of the tumor size on the critical power dissipation, the radius of the tumor was reduced from 18 mm to 1.8 mm while keeping the radius of the healthy tissue ($a = 40$ mm) unchanged. For a temperature condition of T (0.6 mm, 75 s) = 42 °C, the power dissipation was estimated to be $P = 2.3627{\cdot}10^6\mathrm{W/m^3}$, which is around eight times higher than that estimated above for a tumor radius of 18 mm (i.e., $P = 2.9519{\cdot}10^5\mathrm{W/m^3}$). Thus, it appears that the power dissipation density required to raise the cell temperature to an effective treatment range increases as the tumor volume reduces. In other words, as the tumor size decreases, the concentration of magnetic particles required to raise the tumor tissue to an appropriate temperature for therapeutic treatment increases (Kozissnik et al., 2013). Fig. 4 shows the present numerical results for the temperature variation at various locations within the tumor for a power dissipation density of $P =$

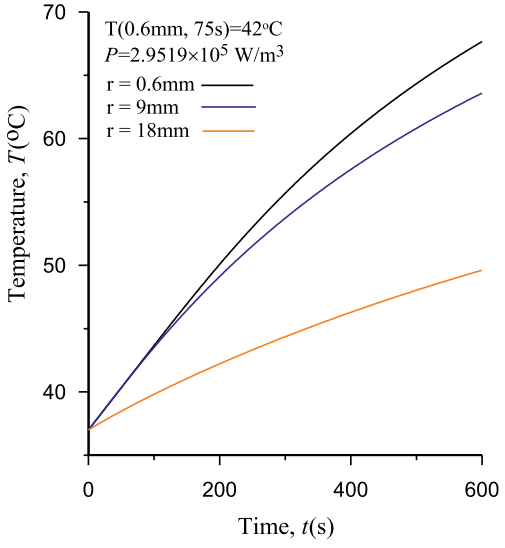

Fig. 3. Numerical results for temperature variation at various locations within tumor given power dissipation of $P = 2.9519{\cdot}10^5\mathrm{W/m^3}$, which is estimated based on T (0.6 mm, 75 s) = 42 °C.

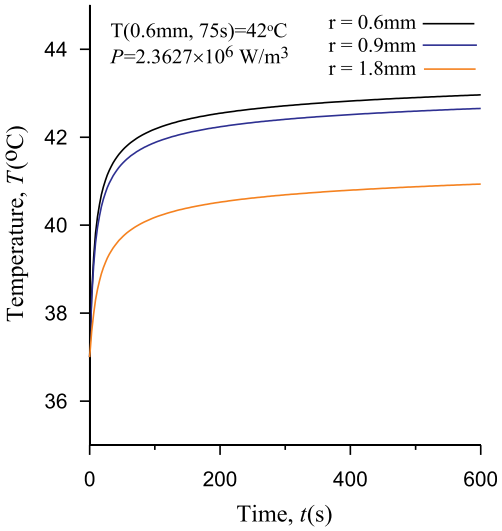

Fig. 4. Numerical results for temperature variation at various locations within tumor given power dissipation of $P = 2.3627{\cdot}10^{6}\mathrm{W/m^3}$, which is estimated for tumor radius of $R = 1.8$ mm and T (0.6 mm, 75 s) = 42 °C.

$2.3627{\cdot}10^{6}\mathrm{W/m^3}$. As time passes, the heat loss through the boundary surface at $r = a$ approaches the sum of the power dissipation and metabolism heat, and hence the temperature distribution in the tumor gradually achieves steady state. From inspection, the temperatures at $r = 0.6$ mm and $r = 1.8$ mm under steady-state conditions ($t = 600$ s) are equal to 42.96 °C and 40.93 °C, respectively.

However, blood perfusion exists in both tumorous and healthy tissue and gives rise to a cooling effect which affects the behavior of the temperature rise in both tissues. Previous research has indicated that the growth of cancer cells can be terminated at temperatures ranging from 42 to 46 °C (Hervault and Thanh, 2014; Chiriac et al., 2015). According to (Wu et al., 2015), the blood perfusion rates are assumed as $w_{b1} = 1.39{\cdot}10^{-2}1/\mathrm{s}$ and $w_{b2} = 6.67{\cdot}10^{-3}1/\mathrm{s}$, respectively, and the power dissipation required to achieve T (0 mm, 600 s) = 46 °C is equal to $P = 5.5242{\cdot}10^{5}\mathrm{W/m^3}$. This power dissipation rate is around 2.5 times higher than that computed in the present study for the case of no blood perfusion (see Fig. 3). Fig. 5 presents the results obtained in the present study for the temperature variation at various points within the tumor ($R = 18$ mm) given the same power density ($P = 5.5242{\cdot}10^{5}\mathrm{W/m^3}$) and blood perfusion rates ($w_{b1} = 1.39{\cdot}10^{-2}1/\mathrm{s}$ and $w_{b2} = 6.67{\cdot}10^{-3}1/\mathrm{s}$) as those considered in (Wu et al., 2015). It is seen that the temperature approaches steady state after just $t = 250$ s. In other words, it can be inferred that blood perfusion removes heat energy from the tissue under the effects of convection heat transfer. After $t = 600$ s, the temperature distribution of the tumor reaches steady state and lies within the range of 41.43–46 °C. In general, the results presented in Figs. 3 and 5 confirm that a larger power density is required to raise the temperature to an effective treatment range when the cooling effects of blood perfusion are taken into account.

4.2. Problem 2

Wu et al., (2015) considered the magnetic hyperthermia problem for the case of a uniform temperature distribution within the target region created by a set of Helmholtz coils. The tumor and normal tissue regions were assumed to have radii of $R = 5$ mm and $a = 10$ mm, respectively. In addition, the material properties and perfusion rates were set as shown in Tables 2 and 3. The dissipation power was not explicitly stated. However, it was reported that the temperature distribution reached steady state after 200 s of excitation and the maximum temperature at the center of the tumor was 43.47 °C. Accordingly, utilizing the numerical method proposed in this study, the power dissipation was inferred as $P = 6.5048{\cdot}10^{5}\mathrm{W/m^3}$ with T (0 mm, 200 s) = 43.47 °C. Fig. 6 shows the numerical results for the time-based temperature variation at various locations within the tumor given an assumed power dissipation of $P = 6.5048{\cdot}10^{5}\mathrm{W/m^3}$. The results show that the temperature at the edge of the normal tissue r = 10 mm is equal to 37 °C. This finding is consistent with the boundary condition given in Eq. (9). However, as shown in Fig. 7 (reproduced directly from Fig. 6 in (Wu et al., 2015)), the calculated value of the boundary temperature was actually slightly higher than this value. In other words, a discrepancy appears in the results presented in (Wu et al., 2015). Notably, this discrepancy is resolved by the numerical method proposed in the present study (see Fig. 6). Fig. 8 shows the results obtained in the present study for the temperature distribution within the tumor considered in (Wu et al., 2015) given the estimated power dissipation density of $P = 6.5048{\cdot}10^{5}\mathrm{W/m^3}$. The results indicate that the temperature within the tumor region lies in the range of 41–44 °C after 150 s of excitation. In other words, the results confirm that a power dissipation density of $P =$

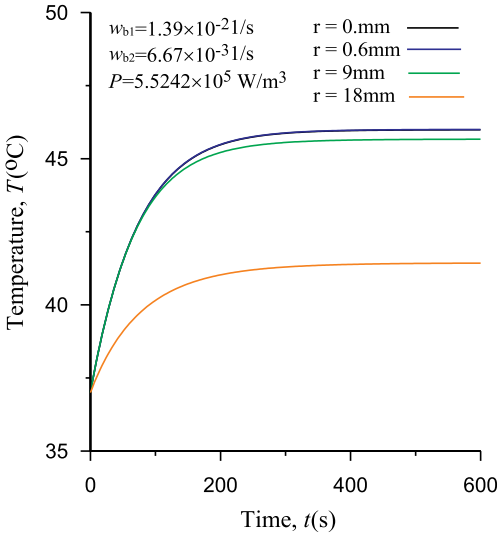

Fig. 5. Numerical results for temperature variation at various locations within tumor given power dissipation of $P = 5.5242{\cdot}10^{5}\mathrm{W/m^3}$, which is estimated for T (0 mm, 600 s) = 46 °C, $w_{b1} = 1.39{\cdot}10^{-2}1/\mathrm{s}$ and $w_{b2} = 6.67 \times 10^{-3}1/\mathrm{s}$.

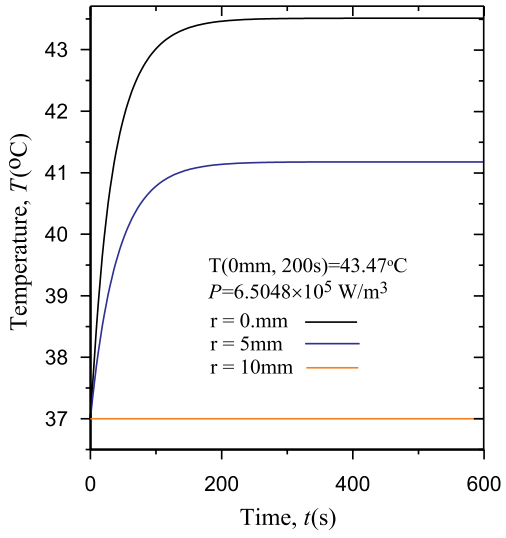

Fig. 6. Numerical results for temperature variation at various locations within tumor for problem considered in (Wu et al., 2015) with power dissipation of $P = 6.5048{\cdot}10^{5}\mathrm{W/m^3}$, which is estimated based on T (0 mm, 200 s) = 43.47 °C.

Table 2
Values of relevant properties for tumor/ferrofluid composite considered in (Wu et al., 2015).

Parameters	Tumor	Magnetite	Composite
Density [kg/m^3]	1060	5180	1070.4
Thermal conductivity [W/m K]	0.55	40	0.552
Specific heat [J/kg K]	3500	4000	3501.5

Table 3
Values of relevant properties for blood and tissue considered in (Wu et al., 2015).

Parameters	Blood innormal tissue	Blood intumor	Normal tissue
Density [kg/m^3]	1000	1000	980
Thermal conductivity [W/m K]	0.512	0.512	0.25
Specific heat [J/kg K]	4180	4180	2300
Perfusion rate [l/s]	6.67×10^{-3}	1.39×10^{-2}	–

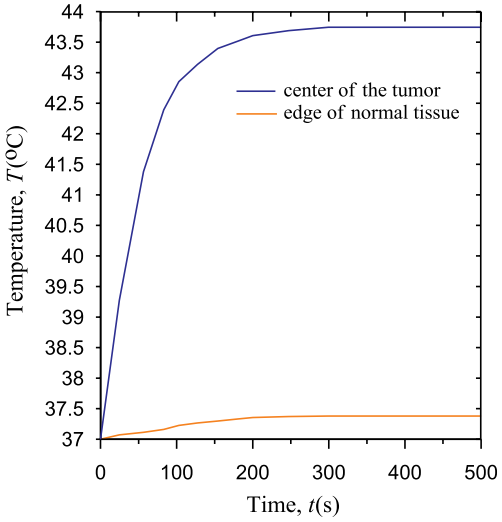

Fig. 7. Temperature variation over time at center and edge of tumor (Note that the figure is reproduced from Fig. 6 in (Wu et al., 2015).).

$6.5048{\cdot}10^5 \mathrm{W/m^3}$ represents an appropriate power density for effective hyperthermia cancer therapy given the tumor conditions assumed in (Wu et al., 2015).

(Thrall et al., 2012) reported that the use of a larger thermal dose to induce a higher temperature is more effective in reducing the tumor volume than a larger magnetic particle volume fraction (with a lower thermal dose). Furthermore, higher temperatures are also beneficial in reducing the heating time required to destroy tumor cells (Silvio and Rudolf, 2013). Accordingly, the present study estimated the power dissipation required to achieve T (5 mm, 75 s) = 41 °C using the proposed numerical method and found a value of $P = 7.4086{\cdot}\ 10^5 \mathrm{W/\ m^3}$. This value is higher than that of $P = 6.5048{\cdot}10^5 \mathrm{W/m^3}$ obtained for T (0 mm, 200 s) = 43.47 °C above, and confirms that a higher power dissipation is required to raise the tumor temperature to a higher temperature range. Figs. 9 and 10 show the temperature profiles within the tumor as a function of the excitation time and location, respectively, for T (5 mm, 75 s) = 41 °C and $P = 7.4086{\cdot}10^5 \mathrm{W/m^3}$. The results confirm that the use of a higher power dissipation density achieves an effective treatment temperature in the range of 41–45 °C after 75 s of excitation without causing any significant damage to the surrounding healthy tissue.

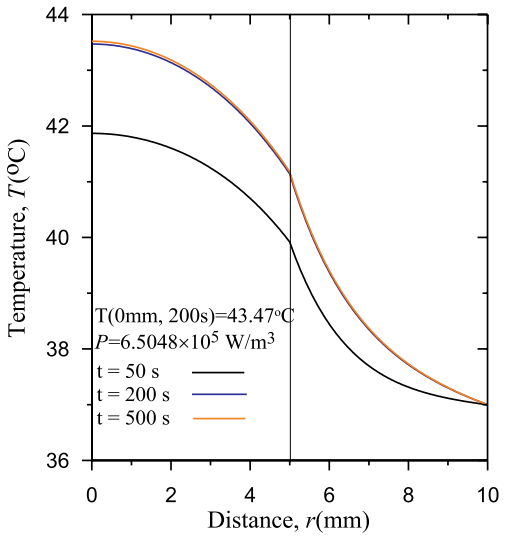

Fig. 8. Numerical results for temperature distribution at various locations within tumor considered in (Wu et al., 2015) with power dissipation of $P = 6.5048{\cdot}10^5 \mathrm{W/m^3}$. (Note that P is estimated based on T (0 mm, 200 s) = 43.47 °C.).

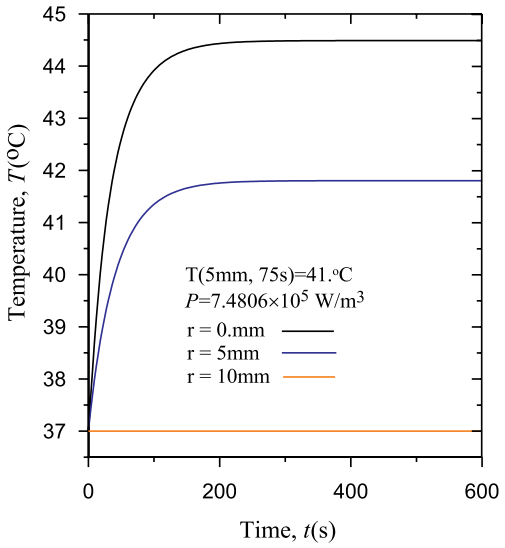

Fig. 9. Numerical results for temperature variation over time within tumor considered in (Wu et al., 2015) with power dissipation of $P = 7.4086{\cdot}10^5 \mathrm{W/m^3}$, which is estimated based on T (5 mm, 75 s) = 41 °C.

5. Conclusions

This study has proposed a numerical method for estimating the power dissipation required to achieve an effective temperature range in the tumor domain for magnetic hyperthermia treatment. The validity of the proposed method has been demonstrated by comparing the results with those obtained analytically. In general, the results have shown that the required power dissipation is related to the rate of temperature rise, the tumor size, the blood perfusion rate, and the tissue properties. In particular, the power dissipation should be increased with an increasing blood perfusion rate and a reducing tumor volume. The proposed method has been used to examine some of the contradictions apparent in the studies of (Tang et al., 2017; Wu et al., 2015). The results have indicated that the present numerical solutions are more reliable than those presented in the literature. The present results have shown that the accuracy of the calculation results is not necessarily improved by

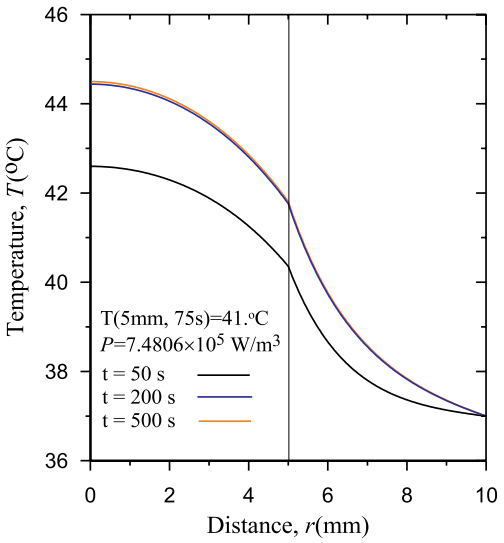

Fig. 10. Numerical results for temperature at various locations within tumor considered in (Wu et al., 2015) with power dissipation of $P = 7.4086 \cdot 10^5 \mathrm{W/m^3}$, which is estimated based on T (5 mm, 75 s) = 41 °C.

increasing the computational complexity (as attempted by Tang et al., (2017)). For ease of comparison and discussion, some of the assumptions made in this study regarding the blood flow and particle distribution are based on those reported in the literature. These assumptions are not necessarily representative of real-world magnetic hyperthermia applications. Nonetheless, the present results and solution procedure are still of significant benefit in conducting future studies using animal or human models.

Acknowledgments

This research was supported by the Ministry of Science and Technology of Taiwan under Grant No. MOST 105-2221-E-269-005-MY2.

References

Bagaria, H.G., Johnson, D.T., 2005. Transient solution to the bioheat equation and optimization for magnetic fluid hyperthermia treatment. Int. J. Hyperth. 21, 57–75.
Chen, K.H., Chen, B.C., Ho, C.Y., 2018. Hyperthermia temperature of magnetic fluid with superparamagnetic nanoparticles subjected to an alternating magnetic field. J. Nanosci. Nanotechnol. 18, 3018–3023.
Chiriac, H., Petreus, T., Carasevici, E., Labusca, L., Herea, D.D., Danceanu, C., Lupu, N., 2015. In vitro cytotoxicity of fe–cr–nb–bmagnetic nanoparticles under high frequency electromagnetic field. J. Magn. Magn. Mater. 380, 13–19.
Cobianchi, M., Guerrini, A., Avolio, M., 2017. Experimental determination of the frequency and field dependence of specific loss power in magnetic fluid hyperthermia. J. Magn. Magn. Mater. 444, 154–160.
Das, P., Colombo, M., Prosperi, D., 2019. Recent advances in magnetic fluid hyperthermia for cancer therapy. Colloids Surf., B 174, 42–55.
Dutta, J., Kundu, B., 2018. Two-dimensional closed-form model for temperature in living tissues for hyperthermia treatments. J. Therm. Biol. 71, 41–51.
Gilchrist, R.K., Medal, R., Shorey, W.D., Hanselman, R.C., Parrott, J.C., Taylor, C.B., 1957. Selective inductive heating of lymphnodes. Ann. Surg. 146, 596–606.
Hedayatnasab, Z., Abnisa, F., Daud, W.M.A.W., 2017. Review on magnetic nanoparticles for magnetic nanofluid hyperthermia application. Mater. Des. 123, 174–196.
Hervault, A., Thanh, N.T.K., 2014. Magnetic nanoparticle-based therapeutic agents for thermo-chemotherapy treatment of cancer. Nano 6 (20), 11553–11573.
Honig, G., Hirdes, U., 1984. A method for the numerical inversion of Laplace transforms. J. Comput. Appl. Math. 10, 113–132.
Johannsen, M., Gneveckow, U., Taymoorian, K., Thiesen, B., Waldofner, N., Scholz, R., 2007. Morbidity and quality of life during thermotherapy using magnetic nanoparticles in locally recurrent prostate cancer: results of a prospective phase I trial. Int. J. Hyperth. 23, 315–323.
Johannsen, M., Thiesen, B., Wust, P., Jordan, A., 2010. Magnetic nanoparticle hyperthermia for prostate cancer. Int. J. Hyperth. 26, 790–795.
Kozissnik, B., Bohorquez, A.C., Dobson, J., Rinaldi, C., 2013. Magnetic fluid hyperthermia: advances, challenges, and opportunity. Int. J. Hyperth. 29, 706–714.
Lahiri, B.B., Muthukumaran, T., Philip, J., 2016. Effect of initial susceptibility and relaxation dynamics on radio frequency alternating magnetic field induced heating in superparamagnetic nanoparticle dispersions. J. Magn. Magn. Mater. 407, 101–113.
Liu, K.C., Cheng, P.J., 2008. Finite propagation of heat transfer in a multilayer tissue. J. Thermophys. Heat Transf. 22, 775–782.
Liu, K.C., Chen, H.T., Cheng, P.J., 2016. Inverse investigation of non-Fourier heat conduction in tissue. J. Therm. Biol. 62, 123–128.
Liu, K.C., Chen, T.M., 2018. Analysis of the thermal response and requirement for power dissipation in magnetic hyperthermia with the effect of blood temperature. Int. J. Heat Mass Transf. 126, 1048–1056.
Lyutyy, T.V., Hryshko, O.M., Yakovenko, M.Yu, 2019. Uniform and nonuniform precession of a nanoparticle with finite anisotropy in a liquid: opportunities and limitations for magnetic fluid hyperthermia. J. Magn. Magn. Mater. 473, 198–204.
Maenosono, S., Saita, S., 2006. Theoretical assessment of FePt nanoparticles as heating elements for magnetic hyperthermia. IEEE Trans. Magn. 42, 1638–1642.
Silvio, D., Rudolf, H., 2013. Magnetic nanoparticle heating and heat transfer on a microscale: basic principles, realities and physical limitations of hyperthermia for tumour therapy. Int. J. Hyperth. 29, 790–800.
Tang, Y., Jin, T., Flesh, R.C.C., 2018. Impact of different infusion rates on mass diffusion and treatment temperature field during magnetic hyperthermia. Int. J. Heat Mass Transf. 124, 639–645.
Tang, Y., Flesch, R.C.C., Jin, T., 2017. Numerical analysis of temperature field improvement with nanoparticles designed to achieve critical power dissipation in magnetic hyperthermia. J. Appl. Phys. 122, 034702.
Thiesen, B., Jordan, A., 2008. Clinical applications of magnetic nanoparticles for hyperthermia. Int. J. Hyperth. 24, 467–474.
Thrall, D.E., Maccarini, P., Stauffer, P., Macfall, J., Hauck, M., Snyder, S., 2012. Thermal dose fractionation affects tumour physiological response. Int. J. Hyperth. 28, 431–440.
Wu, K., Wang, J.P., 2017. Magnetic hyperthermia performance of magnetite nanoparticle assemblies under different driving fields. AIP Adv. 7, 056327.
Wu, L., Cheng, J., Liu, W., Chen, X., 2015. Numerical analysis of electromagnetically induced heating and bioheat transfer for magnetic fluid hyperthermia. IEEE Trans. Magn. 51, 4600204.
Zhou, J.H., Chen, J.K., Zhang, Y., 2007. Theoretical analysis of thermal damage in biological tissues caused by laser irradiation. Mol. Cell. Biomech. 4, 27–39.